An adaptive filtering algorithm in pulse-Doppler radar for counteracting range-velocity jamming

Ahmed Abdalla[a], Mohammed Ramadan[b], Yongjian Liao[b] and Shijie Zhou[b]

[a]College of Electronics and Computer Engineering, Karary University, Omdurman, Sudan; [b]School of Information and Software Engineering, University of Electronic Science and Technology of China, Chengdu, P.R. China

ABSTRACT

In this paper, an anti-jamming scheme based on transmitted multiple pulses through random initial phases and an adaptive iterative filtering algorithm is considered for counteracting range-velocity deceptive jamming in Pulse-Doppler (PD) radar system. This anti-jamming scheme relies on the fact that the digital radio frequency memory (DRFM) repeated jammer needs more than one pulse repetition interval PRI (at least one PRI) to identify the radar transmitted pulses, and therefore uses the captured pulses of the lag PRIs to reproduce multiple false targets. As a consequence, an adaptive-iterative algorithm to estimate the range-Doppler plane of the real targets in range dimension processing and Doppler dimension processing can appropriately suppress the deceptive false targets, which employed the lagged PRIs for the radar deception. Firstly, the proposed method achieves the optimal estimation of the true targets and false targets in the range dimension. Then, with the estimation information in the range dimension, the presented method estimates the range-Doppler plane of the true targets and false targets. Finally, we evaluate the performance of the proposed method as well as achieve a good trade-off between anti-jamming performance and computational complexity via numerical simulations.

KEYWORDS

Anti-jamming; range-velocity jamming; adaptive filter; deceptive jamming; ECCM; pulse-Doppler radar

1. Introduction

With the ability of all-day and all-weather surveillance, radar has got an extensive range of applications and played a significant role in Earth observation, environment monitor, and military reconnaissance fields. Based on the fundamental radar functions, radar systems are widely employed in many practical application areas, both military and civilian (Richards et al., 2010; Yan et al., 2020).

Pulse-Doppler (PD) radar merges the merits of both pulse and continuous wave Doppler radar system, since the transmitted signal is pulsed, the radar can calculate the range, the angle and the elevation similar to the conventional pulsed radar. Besides, PD radar can also calculate the rate of closure, relative to the radar system on a pulse-to-pulse foundation (Kelly, 1986).

CONTACT Yongjian Liao liaoyj@uestc.edu.cn School of Information and Software Engineering, University of Electronic Science and Technology of China, Chengdu, P.R. China

Primarily, Doppler radar is employed for the detection of moving targets whose echo region is much smaller than the relatively stationary clutter return. Moving targets are discriminated from noise, clutter, and jamming on a frequency basis by exploiting the Doppler phenomenon. Conventionally, the pulse-Doppler radar repeats the same waveform to permit efficient pulse compression and Doppler processing technique to be utilised.

Radars are active devices, which use their radio energies to detect the wanted targets. They do not depend on energies that are radiated from the targets themselves. Therefore, in a hostile environment, radar is likely to be subjected to the electronic countermeasures (ECM) to avoid target detection and classification (Wen et al., 2019; H. Yu et al., 2020). ECM system or jammer is usually employed to deny or degrade the ability of the radar system to maintain its mission (Abdalla, Yuan, Longdon et al., 2015). In such situations, the radar will attempt to perform its purpose without being influenced by this attack, which leads to the creation of electronic warfare (EW) (Maini, 2018). ECM and electronic counter-countermeasures (ECCM) form the principal conflicting pair in modern electronic warfare (Abdalla et al., 2017; Haykin, 2006). By the mean of precise replication and reproduction of the radar signal through the digital radio frequency memory (DRFM), the modern deception ECM has entered an area of coherent false targets. From the point view of the radar, such false targets can easily obtain radar coherent processing gain, such that they are capable of affecting or even screen the detection and extraction of true targets stealthily (Berger, 2003; Bokov et al., 2019; W. Liu et al., 2019; Mesarcik et al., 2019; G. Zhang et al., 2019). Moreover, the pressed parameters extracted by subsequent processes can further consume the resources of radar and protect true targets, and as a result, an error decision may be made about the current target or air intelligence. It is a powerful technology measure to counter various types of radars, especially advanced radar systems.

In PD radar the conventional pulse compression method is a matched filter, which is becoming useless in the presence of modern electronic warfare scenarios, especially the active deceptive jamming. Accordingly, several anti-jamming methods are presented to decrease or remove the impact of active deceptive jamming. Most of these methods exploit the fact that the DRFM would need more than one PRI to study the transmit signal. Thus, radar can employ different pulses at a PRI level to counter DRFM jamming. Owing to the pulse difference at the PRI level, the received signal from the desired targets and the DRFM jamming might have different signatures that could be exploited to distinguish between the targets and jamming through a suitable signal processing algorithm.

Extensive strategies have been done on the ECCM to counteract deceptive jamming, such as pulse diversity methods (Abdalla, Yuan et al., 2016; Akhtar, 2009), coherent clustering (Ahmed et al., 2018) and data fusion methods (Bandiera et al., 2008; Zhu, 2020). Nevertheless, they are not accessible for PD radar, since the ECCM ability is limited to a one-dimensional view. In (Xiong et al., 2016; J. Zhang et al., 2013) transmitting pulses with random initial phases in the PRI domain against velocity deception jamming has been presented. Nevertheless, these methods are limited to the constraint of the single target circumstances.

The frequency diverse array multi-input-multi-out-put (FDA-MIMO) radar to counteract the jamming in the joint transmit-receive domain has been examined in (Xu et al., 2018). Furthermore, a method based on subarray FDA signal processing is projected to defeat deceptive ECM signals (Xiong et al., 2016).However, the performance will deteriorate strictly as the ranges of the false and true targets are close.

In pulse-Doppler radar, many deceptive jamming suppression works have been investigated to counter the velocity deceptive jamming. In (Abdalla et al., 2016), an anti-velocity deception jamming via pulses with adaptive initial phases for one target scenario is considered. An effective cognitive waveform design method with adaptive initial phases has been addressed in (Xu et al., 2018) to counteract the velocity deception jamming. Thus, a multichannel processing deception with different integral multiple PRI delay is utilised to estimate the parameters of the true and false targets. In the paper proposed by Yang et.al (2015), an effective method has been provided to encounter the effect of velocity deception jammer in the multi-target scenario. This method has highlighted the desired waveform according to the estimation of a rough frequency range of the real and false targets. Additionally, the method has analysed the different spectral characteristics of real and false targets. Then, a modified Newton algorithm has been used for the optimising problem to produce a waveform that has improved performance. With the optimised waveform, the repeated DRFM jammer generates notches around real targets in the frequency domain, which separates the real targets and the false targets successfully.

Cui et al. (2017) proposed an adaptive sequential estimation algorithm for velocity jamming suppression. This method focuses on an alternative processing strategy. Particularly, it considers a monostatic PD radar system which transmits a train consisting of several pulses with random initial phases. Moreover, the method assumes that the DRFM jammer requires more than one PRIs to distinguish the radar transmit pulses, and then utilises the captured pulses to generate multiple false targets. An adaptive sequential estimation method is provided to achieve simultaneously the target and jamming profiles in Doppler domains in an iterative manner, which declares that the velocity jamming is satisfactorily removed in the target profile.

It is worth noting that most of the methods in PD radar deal with the velocity deception jamming. However, as to range-velocity deception jamming, which is more powerful to deceive the victim radar, there are few methods presented. Zhang et al. (2016) proposed and studied the range-velocity jamming suppression method based on the adaptive iterative filtering algorithm, but the suppressing performance has not been well evaluated and compared with the existing works.

Z. Liu et al. (2018)proposed an algorithm focuses on developing an anti-velocity jamming strategy that enhances the ability of a PD radar to detect moving targets in the presence of translational and/or micro motion velocity jamming. The strategy adopts random pulse initial-phase pulses as its transmitted signal and thus gets DRFM jammers not adaptable to the randomness of initial phase of the transmitted pulses in the PRI domain. The dissimilarity between the true target echo and the false target jamming signal at each PRI is then used to distinguish the true and false target signals.

The work presented in (Mandal & Mishra, 2017), used a reformulated LMS algorithm-based pipelined architecture of adaptive transversal equaliser that used coordinate rotation digital computer (CORDIC), which is hardware-efficient iterative method, which uses rotations to calculate a wide range of elementary functions a main processing element to update angles instead of filter coefficients.

Yi Yu a (Liang et al., 2011), proposed and analysed the sparsity-aware sign subband adaptive filtering with individual weighting factors (S-IWF-SSAF) algorithm, and consider its application in acoustic echo cancellation (AEC). The proposed method realised by incorporating the sparsity-aware technique, to propose the S-IWF-SSAF algorithm, and analyse its performance in-depth in impulsive noise. In (Z. Liu et al., 2018), a new elevation and azimuth direction finding method is developed to overcome the mutual coupling and the failure in pairing can cause severe performance degradation difficulties in the L-shaped array configuration in two-dimensional (2-D) directions-of-arrival (DOA) estimation problem.

This paper aims to present an ECCM method in monostatic PD radar to counter the range-velocity jamming. The proposed method transmits multiple pulses with random initial phases and supposes that the DRFM jammer needs i PRIs to identify the radar transmit pulses, and then utilises the captured pulses to create false targets. Therefore, an adaptive iterative estimation algorithm is utilised to estimate the range-Doppler plane of the true targets and false targets, respectively. Thus, with the estimation of the range-Doppler plane of both true and false targets, the false targets can be suppressed and the true targets are maintained.

The rest of this paper organised as follows. In Section 2, the signal model in the range-velocity deceptive jamming scenario is presented. In Section 3, the detailed description of our adaptive filtering method is proposed which includes the estimation of the received signal in both range dimension and Doppler dimension. Our simulation results are discussed in Section 4 to clarify the validity of the proposed method. Finally, the conclusion of our work is drawn in Section 5.

2. Signal model in the range-velocity deceptive jamming scenario

Let consider a mono-static pulse-Doppler radar, which transmits M coherent train pulses. Let $s_m(t- mT)$ denotes the baseband complex envelope of the m-th transmitted pulse, where T represents the PRI. In the absence of the active deceptive jamming, the PD radar is served to detect K-th real targets in the surveillance region. Thus, the received signal in a jamming-free scenario at the m-th can be represented as:

$$x_m(t) = R_m(t) + n_m(t) \tag{1}$$

Where $n_m(t)$ denotes the corresponding noise, which is often assumed to be the AWGN and $R_m(t)$ is the received echo, which can be shown as:

$$\begin{gathered} R_m(t) = \sum_{k=1}^{K} \sigma_R^k \exp(j2\pi m f_R^k) s_m(t - \tau_R^k - mT) + n_m(t) \\ m = 1, \cdots, M+1 \end{gathered} \tag{2}$$

Where τ_R^k denotes the time delay of the k-th real target, σ_R^k denotes the complex amplitude of the k-th true target, and f_R^k denotes the normalised Doppler frequency of the k-th real target which expressed as $f_R^k = 2v_R^k T/\lambda$, in which v_R^k is the velocity (radial velocity) and is the λ wavelength.

In the absence of the active jamming, the PD radar can proficiently detect the real targets with high performance. However, in the presence of active deceptive jamming, the PD radar suffers a serious threat that degrades the radar performance significantly. It is worth remarking that the proposed method assumed that the DRFM repeated jammer lagged i PRIs (in this method is assumed to be one PRI) behind the radar as can be shown in Figure 1. Further, it assumed that L-th range-velocity deceptive false targets are created to deceive the PD radar.

Generally, because the pulse signal is processed in baseband, the signal sampling rate is then relatively at a lower level. Some methods confirmed that the error introduced by the time delay difference is likely less than the error introduced in the sampling process. Hence, this error can be completely neglected on such conditions. In some exceptional cases, the time-delay difference of each interesting arrival pulse cannot be simply neglected. Under this condition, it must be compensated. Some methods use a technique to compensate the motion, based on shifting the matching weight coefficients. It is useful when the signal bandwidth is much wider and the target velocity is much higher. For simplicity, some methods assumed that the time-delays associated with reflectors are more liable to minor alterations across slow-time positions and can be modelled with a linearly increasing offset as a function of time.

In our proposed method, two-dimensional frequency domain motion compensation algorithm is used to overcome the limitation of one-dimensional range frequency domain motion compensation and match filtering a technique to compensate the motion, based on shifting the matching weight coefficients. Thus, the received signal can be rewritten as:

$$x_m(t) = R_m(t) + D_m(t) + n_m(t) \tag{3}$$

The deceptive jamming signal $D_m(t)$ can be illustrated similarly to the true targets, but with a difference in the transmitted pulse that the PD radar has transmitted at the previous PRI, thus, $D_m(t)$ can be expressed as..

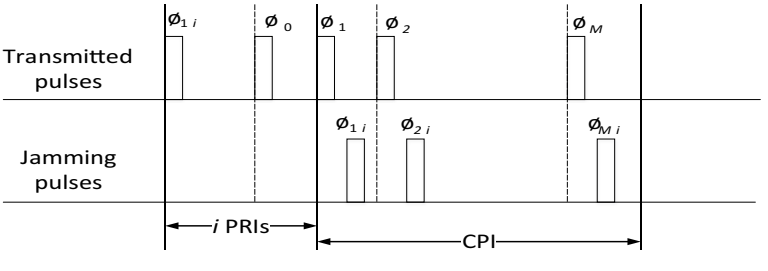

Figure 1. Scheme of transmitting pulses with random initial phases in CPI with lag i PRIs.

$$D_m(t) = \sum_{l=1}^{L} \sigma_D^l \exp(j2\pi m f_D^l) s_{m\ \ i}(t - \tau_D^l - mT) \quad m = 1, \cdots, M \tag{4}$$

Where τ_D^l, σ_D^l and f_D^l represent the complex amplitude, time delay, and Doppler frequency of the l-th false target, respectively.

The received signal Equation (3) can be recast as:

$$\begin{aligned} x_m(t) &= R_m(t) + D_m(t) + n_m(t) \\ x_m(t) &= \sum_{k=1}^{K} \sigma_R^k \exp(j2\pi m f_R^k) s_m(t - \tau_R^k - mT) \\ &\quad + \sum_{l=1}^{L} \sigma_D^l \exp(j2\pi m f_D^l) s_{m\ \ i}(t - \tau_D^l - mT) + n_m(t) \end{aligned} \tag{5}$$

For simplicity, this method deals with the last M pulses in one CPI. Furthermore, the impact of the Doppler Effect within the pulses is ignored.

The received signal after sampling at a fast time can be expressed in vector form as:

$$\mathbf{x}_m = [x_m[1], x_m[2], \cdots, x_m[Z-1], x_m[Z]]^T \tag{6}$$

Where Z represents the length of the range cell, $\mathbf{X}[z] = [x_1, x_2, \cdots, x_{M\ \ 1}, x_M]^T$ is the sampling result of the M received pulses. Noteworthy, the discrete form of $s_m(t)$ for the true targets can be expressed by the $s_m = [s_m(1), s_m(1), \cdots, s_m(G-1), s_m(G)]^T$. The m-th pulses from the true targets are termed as $s_{R,m}(t)$, while the m-th pulses from the deceptive false targets are termed as $s_{D,m}$, in which $s_{D,m} = s_{R,m\ \ i}$.

It is worth noting that, we let G be the range cell that begins at the z-th range cell and can be written as $\mathbf{x}_m[z] = [x_m[z], x_m[z+1], \cdots, x_m[z+(G-2)], x_m[z+(G-1)]$. Moreover, U represents the total number of the sampling points in the normalised Doppler frequency. In doing so, the vector $\mathbf{f} = [f_1, f_2, \cdots, f_{U\ \ 1}, f_U]$ contains all the sampling values of the normalised Doppler frequency, where $f_u = (u-1)/U, (u = 1, \cdots, U)$. Thus, for the range profiles of the G – 1 range cells, which lie before and after the z-th range cell of the true target and the deceptive false target in the frequency of f_u, and they can be expressed respectively for true targets and deceptive false targets as:

$$\mathbf{A}_R[z](f_u) = [A_R[z-(G-1), u], \cdots, A_R[z+(G-1), u]]^T \tag{7}$$

And

$$\mathbf{A}_D[z](f_u) = [A_D[z-(G-1), u], \cdots, A_D[z+(G-1), u]]^T \tag{8}$$

From the above analysis, the total received signal Equation (5) can be written in discrete form as..

$$
\begin{aligned}
x_m[z] &= R_m[z] + D_m[z] + n_m[z] \\
x_m[z] &= B_{R,m} \sum_{u=1}^{U} \mathbf{A}_R[z](f_u) \exp(j2\pi m f_u) \\
&\quad + B_{D,m} \sum_{u=1}^{U} \mathbf{A}_D[z](f_u) \exp(j2\pi m f_u) + n_m[z]
\end{aligned} \tag{9}
$$

Where the AWGN $n_m[z]$ has a unit of power of the m-th pulse. Moreover, $B_{R,m}$ and $B_{D,m}$ represent the fast time transformation matrices of the m-th omitted pulse of the true targets and the deceptive false targets respectively. The term $B_{R,m}$ can be expressed as:

$$
B_{R,m} = \begin{pmatrix}
s_{R,m}(G) & s_{R,m}(G-1) & \cdots & s_{R,m}(1) & & \\
 & s_{R,m}(G) & \cdots & s_{R,m}(2) & s_{R,m}(1) & \\
 & & \ddots & \vdots & \vdots & \ddots \\
 & & & s_{R,m}(G) & \cdots & \cdots & s_{R,m}(1)
\end{pmatrix} \tag{10}
$$

Similarly $B_{D,m}$ can be expressed as:

$$
B_{D,m} = \begin{pmatrix}
s_{D,m}(G) & s_{D,m}(G-1) & \cdots & s_{D,m}(1) & & \\
 & s_{D,m}(G) & \cdots & s_{D,m}(2) & s_{D,m}(1) & \\
 & & \ddots & \vdots & \vdots & \ddots \\
 & & & s_{D,m}(G) & \cdots & \cdots & s_{D,m}(1)
\end{pmatrix} \tag{11}
$$

In Equation (9) the summation operation in the part of the true target can be rewritten as below:

$$
\sum_{u=1}^{U} \mathbf{A}_R[z](f_u) \exp(jmf_u) = [\mathbf{A}_R[z](f_1), \cdots, \mathbf{A}_R[z](f_u)] \begin{bmatrix} \exp(j2\pi m f_1) \\ \exp(j2\pi m f_2) \\ \vdots \\ \exp(j2\pi m f_u) \end{bmatrix} \tag{12}
$$

Analogously, for the deceptive false targets can be rewritten as:

$$
\sum_{u=1}^{U} \mathbf{A}_D[z](f_u) \exp(jmf_u) = [\mathbf{A}_D[z](f_1), \cdots, \mathbf{A}_D[z](f_u)] \begin{bmatrix} \exp(j2\pi m f_1) \\ \exp(j2\pi m f_2) \\ \vdots \\ \exp(j2\pi m f_u) \end{bmatrix} \tag{13}
$$

Where the vector $\mathbf{f}_m = [\exp(j2\pi m f_1), \exp(j2\pi m f_2), \cdots, \exp(j2\pi m f_u)]^T$ is the Doppler phase of true and false targets.

Let $\mathbf{A}_{R,D}[z]$ represents the range-Doppler plane sampling result which begins from the z-(G-1)-th range cell to the z+(G-1)-th range cell of both the true target and the deceptive false target, specifically

$$\mathbf{A}_{R,D}[z] = [\mathbf{A}_{R,D}[z](f_1), \mathbf{A}_{R,D}[z](f_2), \cdots, \mathbf{A}_{R,D}[z](f_U)]$$

$$\mathbf{A}_{R,D}[z] = \begin{pmatrix} \mathbf{A}_{R,D}[z-(G-1),1] & \mathbf{A}_{R,D}[z-(G-1),2] & \cdots & \mathbf{A}_{R,D}[z-(G-1),U] \\ \mathbf{A}_{R,D}[z-(G-2),1] & \mathbf{A}_{R,D}[z-(G-2),2] & \cdots & \mathbf{A}_{R,D}[z-(G-1),U] \\ \vdots & \vdots & \ddots & \vdots \\ \mathbf{A}_{R,D}[z+(G-1),1] & \mathbf{A}_{R,D}[z+(G-1),2] & \cdots & \mathbf{A}_{R,D}[z+(G-1),U] \end{pmatrix} \tag{14}$$

In Equation (14), the column of $\mathbf{A}_{R,D}[z]$ is the sampling result in the range dimension of a specified Doppler frequency, whereas the row indicates the sampling result in the Doppler dimension of a specified range cell.

Therefore, m-th received pulse can be interpreted as the linear transformation of rows and columns of both $\mathbf{A}_R[z]$ and $\mathbf{A}_D[z]$. Thus, Equation (9) can be written as:

$$x_m[z] = \{B_{R,m}\mathbf{A}_R[z] + B_{D,m}\mathbf{A}_D[z]\}\mathbf{f}_m + n_m[z] \tag{15}$$

Equation (15) demonstrates the relationship between the transmitted signal, the received signal, and the range-Doppler plane of both the true targets and the deceptive false targets. As mentioned above, the m-th received pulse is the sum of the linear transformation of $\mathbf{A}_R[z]$ and $\mathbf{A}_D[z]$. Namely, the transformation is accomplished in the fast-time dimension to the rows of $\mathbf{A}_R[z]$ and $\mathbf{A}_D[z]$, as well as in the slow-time dimension to the columns of $\mathbf{A}_R[z]$ and $\mathbf{A}_D[z]$.

Ultimately, the whole range-Doppler plane sampling result of the real targets and the deceptive false targets $\mathbf{A}_{R,D}[z]$ can be summarised as:

$$\mathbf{A}_{R,D} = \begin{pmatrix} \mathbf{A}_{R,D}[1,1] & \mathbf{A}_{R,D}[1,2] & \cdots & \mathbf{A}_{R,D}[1,U] \\ \mathbf{A}_{R,D}[2,1] & \mathbf{A}_{R,D}[2,2] & \cdots & \mathbf{A}_{R,D}[2,U] \\ \vdots & \vdots & \ddots & \vdots \\ \mathbf{A}_{R,D}[Z,1] & \mathbf{A}_{R,D}[Z,2] & \cdots & \mathbf{A}_{R,D}[Z,U] \end{pmatrix} \tag{16}$$

3. The proposed adaptive filtering method

This section is devoted to the estimation of the range-Doppler plane to effectively suppress the deceptive false targets from the true targets through the adaptive iterative filtering algorithm and benefitting from the transmitted pulses of the current and previous PRIs. The method of two-stage processing is known as a modified adaptive multi-pulse compression (MAMPC) algorithm that was firstly used for suppressing the range-Doppler side-lobes in (Abdalla et al., 2016) and extended in (Yang, Cui et al., 2015) for clutter suppression but without the variation of the initial phases of the transmitted pulses. Thus, the iteration of the proposed method is divided into two stages, which includes the process for the rows (Doppler dimension) and columns (range dimension) sequentially.

3.1. Estimating the received signal in range dimension

Herein, the processing of the range dimension is provided. Let $\psi_{R,m}[z] = \mathbf{A}_R[z]\mathbf{f}_m$ and $\psi_{D,m}[z] = \mathbf{A}_D[z]\mathbf{f}_m$ represent $(2G - \ 1)$ the range profile estimation of the range cells, which centre on the z-th range cell equivalent to the m-th pulse. $\psi_{R,m}[z]$ and $\psi_{D,m}[z]$ can be respectively recast as:

$$\psi_{R,m}[z] = [\psi_{R,m}[z-(G-1),\cdots,\psi_{R,m}[z+(G-1)]]^T \tag{17}$$

$$\psi_{D,m}[z] = [\psi_{D,m}[z-(G-1),\cdots,\psi_{D,m}[z+(G-1)]]^T \tag{18}$$

Then, by substituting the above two equations in the m-th received, Equation (15) can be rewritten as:

$$x_m[z] = B_{R,m}\psi_{R,m}[z] + B_{D,m}\psi_{D,m}[z] + n_m[z] \tag{19}$$

Therefore, for the m-th received pulse in range profile, the method needs to estimate the $\psi_{R,m}[z]$ firstly with estimation processing corresponding to the optimisation problem, which can formulate for $z = G,\cdots,Z-(G-1)$ as follows:

$$\begin{cases} [\min \quad E\left[|\mathbf{w}_{R,m}[z]^H x_m[z]|^2\right] \\ s.t.: |\mathbf{w}_{R,m}[z]^H s_{R,m} = 1 \\ z = G,\cdots,Z-(G-1) \end{cases} \tag{20}$$

Let suppose that the estimation method iterated Q times. More precisely, the Q iterations start for q = 1 to q = Q, which the q-th iteration satisfied $(1 \le q \le Q)$.

According to both Ref (Yang, Cui et al., 2015) and Ref (S. Zhang et al., 2016), the coefficients of the estimation filtering can be expressed as:

$$\mathbf{w}_{R,m}^{(q)}[z] = \frac{\left(\xi[z]^{(q\ \ 1)}\right)^{\ 1} s_{R,m}}{s_{R,m}^H \left(\xi[z]^{(q\ \ 1)}\right)^{\ 1} s_{R,m}} \tag{21}$$

Where $\xi[z]^{(q\ \ 1)}$ can be interpreted as:

$$\xi[z]^{(q\ \ 1)} = B_{R,m}\,\Pi_{R,m}^{(q\ \ 1)}[z]\,B_{R,m}^H + B_{D,m}\,\Pi_{D,m}^{(q\ \ 1)}[z]\,B_{D,m}^H + I \tag{22}$$

In which, $\Pi_{R,m}^{(q\ \ 1)}[z] = diag(|\psi_{R,m}^{(q\ \ 1)}[z-(G-1)]|^2,\cdots,|\psi_{R,m}^{(q\ \ 1)}[z+(G-1)]|^2)$, similarly, $\Pi_{D,m}^{(q\ \ 1)}[z] = diag(|\psi_{D,m}^{(q\ \ 1)}[z-(G-1)]|^2,\cdots,|\psi_{D,m}^{(q\ \ 1)}[z+(G-1)]|^2)$ and I is an identity matrix. Moreover, the range profile estimation result can be shown as:

$$\begin{aligned} &\psi_{R,m}^{(q)}[z] = (\mathbf{w}_{R,m}^{(q)}[z])^H x_m[z] \\ &\psi_{R,m}^{(q)}[z] = \frac{s_{R,m}^H \left(\xi[z]^{(q\ \ 1)}\right)^{\ 1} x_m[z]}{s_{R,m}^H \left(\xi[z]^{(q\ \ 1)}\right)^{\ 1} s_{R,m}} \\ &z = G,\cdots,Z-(G-1) \end{aligned} \tag{23}$$

For $z = 1,\cdots,G-1$, the optimisation criteria can be formulated as..

$$\begin{cases} [\min \quad E\left[|\mathbf{w}_{R,m}[z]^H x_m[z]|^2\right] \\ s.t.: |\mathbf{w}_{R,m}[z]^H b_{R,m,z} = 1 \\ z = 1, \cdots, (G-1) \end{cases} \tag{24}$$

Where $b_{R,m,z}$ denotes the z-th column of $B_{R,m}$, which its range profile estimation can be shown as:

$$\begin{aligned} \psi_{R,m}^{(q)}[z] &= \frac{b_{R,m,z}^H \{\xi[G]^{(q\ \ 1)}\}^{\ \ 1} x_m[G]}{b_{R,m,z}^H \{\xi[G]^{(q\ \ 1)}\}^{\ \ 1} b_{R,m,z}} \\ z &= 1, \cdots, (G-1) \end{aligned} \tag{25}$$

For $z = Z-(G-2), \cdots, Z$ the optimisation problem can be given by:

$$\begin{cases} [\min \quad E\left[|\mathbf{w}_{D,m}[z]^H x_m[z-(G-1)]|^2\right] \\ s.t.: |\mathbf{w}_{D,m}[z]^H b_{D,m,z\ \ Z+(2G\ \ 1)} = 1 \\ z = Z-(G-2), \cdots, Z \end{cases} \tag{26}$$

The range profile estimation result can be shown as:

$$\begin{aligned} \psi_{R,m}^{(q)}[z] &= \frac{b_{R,m,z\ \ Z+(2G\ \ 1)}^H \{\xi[Z-(G-1)]^{(q\ \ 1)}\}^{\ \ 1} x_m[Z-(G-1)]}{b_{R,m,z\ \ Z+(2G\ \ 1)}^H \{\xi[Z-(G-1)]^{(q\ \ 1)}\}^{\ \ 1} b_{R,m,z\ \ Z+(2G\ \ 1)}} \\ z &= Z-(G-2), \cdots, Z \end{aligned} \tag{27}$$

Accordingly, the estimations achieved in Equations (23), (25) and (27) require the received signal waveform of the true targets and the deceptive false targets to be known to estimate the range profile of the true targets $\psi_{R,m}[z]$. Moreover, prior information on both the true targets and the deceptive false targets range profile also needs to be known. Thus, the proposed method can estimate the range profile of the deceptive false targets with similar derivations that used for the true targets range profile, which can be obtained as follows:

$$\begin{aligned} \psi_{D,m}^{(q)}[z] &= \frac{s_{D,m}^H \left(\xi[z]^{(q\ \ 1)}\right)^{\ \ 1} x_m[z]}{s_{R,m}^H \left(\xi[z]^{(q\ \ 1)}\right)^{\ \ 1} s_{R,m}} \\ z &= G, \cdots, Z-(G-1) \end{aligned} \tag{28}$$

$$\begin{aligned} \psi_{D,m}^{(q)}[z] &= \frac{b_{D,m,z}^H \{\xi[G]^{(q\ \ 1)}\}^{\ \ 1} x_m[G]}{b_{D,m,z}^H \{\xi[G]^{(q\ \ 1)}\}^{\ \ 1} b_{D,m,z}} \\ z &= 1, \cdots, (G-1) \end{aligned} \tag{29}$$

$$\begin{aligned} \psi_{D,m}^{(q)}[z] &= \frac{b_{D,m,z\ \ Z+(2G\ \ 1)}^H \{\xi[Z-(G-1)]^{(q\ \ 1)}\}^{\ \ 1} x_m[Z-(G-1)]}{b_{D,m,z\ \ Z+(2G\ \ 1)}^H \{\xi[Z-(G-1)]^{(q\ \ 1)}\}^{\ \ 1} b_{D,m,z\ \ Z+(2G\ \ 1)}} \\ z &= Z-(G-2), \cdots, Z \end{aligned} \tag{30}$$

3.2. Estimating the received signal in Doppler dimension

Secondly, after estimating the received signal in the range dimension, the estimation in Doppler processing is needed to achieve the whole range-Doppler plane. Accordingly, the Doppler estimation is carried out for every range cell using the range profile that has been estimated for both the true targets and the deceptive false targets, which can be termed as:

$$\Theta_{D,R}^{(q)}[z] = [\psi_{D,R,1}^{(q)}[z] \ , \psi_{D,R,2}^{(q)}[z] \ , \cdots , \psi_{D,R,M}^{(q)}[z]] \tag{31}$$

Moreover, let:

$$\mathbf{F} = [\mathbf{f}_1, \mathbf{f}_2, \cdots, \mathbf{f}_M] \tag{32}$$

Then, according to Ref (S. Zhang et al., 2016) and based on the received signal Equation (5) the estimated $\Theta_{D,R}^{(q)}[z]$ can be expressed with the whole range-Doppler plane as:

$$\Theta_{D,R}^{(q)}[z] = \mathbf{A}_{D,R}^{(q)}[z] \ \mathbf{F} + \hat{N}[z] \tag{33}$$

Where $\hat{N}[z]$ denotes the i.i.d unit power AWDN estimated error vector.Equation (33) can be rearranged and rewritten as:

$$(\Theta_{D,R}^{(q)}[z])^H = \mathbf{F}^H (\mathbf{A}_{D,R}^{(q)}[z])^H + (\hat{N}[z])^H \tag{34}$$

Therefore, using similar mathematical derivation in Equation (19), the range-Doppler plane estimation can be expressed as:

$$\begin{aligned} &\mathbf{A}_{D,R}^{(q)}[z,u] = \frac{\mathbf{F}_u^H \{\mathbf{F}\mathbf{D}_{R,D}^{q\ 1}[z]\mathbf{F}^H + I/s_m^H s_m\}^{\ 1} \eta_{R,D}^q[z]}{\mathbf{F}_u^H \{\mathbf{F}\mathbf{D}_{R,D}^{q\ 1}[z]\mathbf{F}^H + I/s_m^H s_m\}^{\ 1} \mathbf{F}_u^H} \\ &u = 1, 2, \cdots, U \\ &z = 1, 2, \cdots, Z \end{aligned} \tag{35}$$

Where $\mathbf{F}_u$ denotes the i-th row of $\mathbf{F}$, $\eta_{R,D}^q[z]$ denotes z-th column of $(\Theta_{D,R}^{(q)}[z])^T$ and $\mathbf{D}_{R,D}^{q\ 1}[z]$ can be expressed as: $\mathbf{D}_{R,D}^{q\ 1}[z] = diag(|\mathbf{A}_{R,D}^{q\ 1}[z,1]|^2, |\mathbf{A}_{R,D}^{q\ 1}[z,2]|^2, \cdots, |\mathbf{A}_{R,D}^{q\ 1}[z,U]|^2$.

It is worth noting that, after estimating the range-Doppler plane the true targets and the deceptive false targets can be easily distinguished according to their difference in the initial phase from different PRIs. The processing steps for suppressing the deceptive false targets can be summarised as below:

- Transmit pulses with random initial phases as shown in Figure (1).
- Receive the signal in the deceptive jamming scenario.
- Deal with the last received M pulses in one CPI.
- Obtain the whole range-Doppler plane sampling results of both the real targets and the deceptive false targets $\mathbf{A}_{R,D}[z]$ using Equation (16)) at q = 0.
- Adaptive-iterative estimation f iltering in range-dimension to obtain $\psi_{R,m}[z]$ and $\psi_{D,m}[z]$ using Equation (27) and (30) respectively.
- Adaptive-iterative estimation f iltering in Doppler-dimension to get the range-Doppler plane $\mathbf{A}_{D,R}^{(q)}[z, u]$ based on the estimated $\psi_{R,m}[z]$ and $\psi_{D,m}[z]$ using Equation (35).

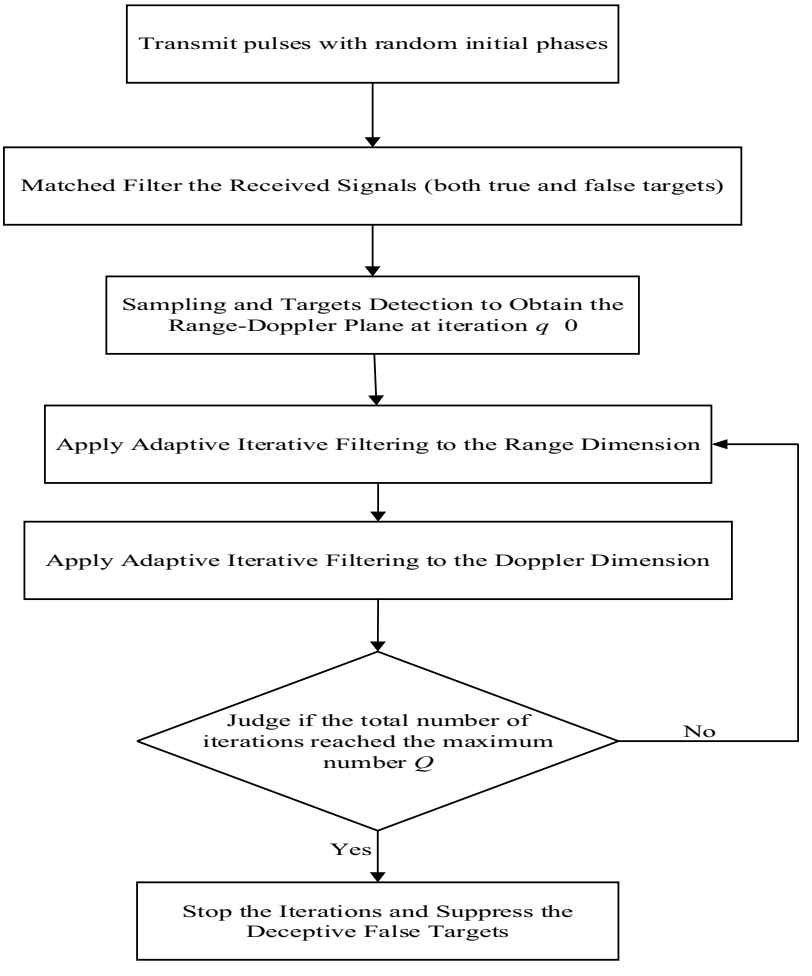

Figure 2. Working flow for countering the range-velocity deceptive jamming.

- Stop the iterations and exist when the total number of iterations reached the maximum number Q.

The working flow of PD radar for countering range-velocity deception jamming using the proposed method is explained in Figure 2.

4. Simulation results and discussion

This subsection is dedicated to numerical simulations of the presented method. To this end, a PD radar system transmitted signal with random initial phases is considered. The transmitted signal is LFM phase coding with code length chooses to be (M = 32). The central frequency fc = 1.2 GHz, the PRI = 1 ms, and the power of the (AWGN = 1). In particular, the simulation assumes in the surveillance area there are K-th true targets and L-th false targets satisfy the Swerling-0 model, in which the false targets lag one PRI behind the true targets (i = 1). Tables 1 and 2 provide the parameters of the true and the

false targets respectively. Besides, the sampling number in the range and Doppler dimensions are assumed to be G = 32 and U = 128 respectively, whereas the total number of range cells in the range-Doppler domain is assumed to be Z = 100. Finally, the exit of the adaptive iterations is set to be Q = 8.

Firstly, the estimated range-Doppler plane using the conventional matching filtering-moving target detection (MTD) and Doppler processing is demonstrated in Figure 3. It is clear to see that from Figure 3, the traditional matching filtering- MTD and Doppler processing method cannot successfully recognise the true targets, and failed to detect and estimate the range-Doppler plane of the true and the false targets correctly. This is due to the high range-Doppler side-lobes and the cross-correlation side-lobes introduced by the jamming signals (Yang, Li et al., 2015; X. Yu et al., 2018).

Table 1. The parameters of the true targets.

Target	Range Cell Index	Velocity (m/s)	Doppler Frequency	Amp(dB)
1	30	30	0.2	5
2	35	20	0.133	−2
3	45	−40	−0.267	10
4	52	25	0.167	0
5	60	45	0.3	8
6	65	−20	−1.33	6
7	75	50	0.333	3
8	83	62	0.413	−5

Table 2. The parameters of the deceptive false targets.

Target	Range Cell Index	Velocity (m/s)	Doppler Frequency	Amp(dB)
1	10	40	0.267	20
2	25	25	0.167	30
3	40	−64	−0.427	40
4	60	62	0.413	15
5	55	−35	−0.233	32
6	70	50	0.333	25

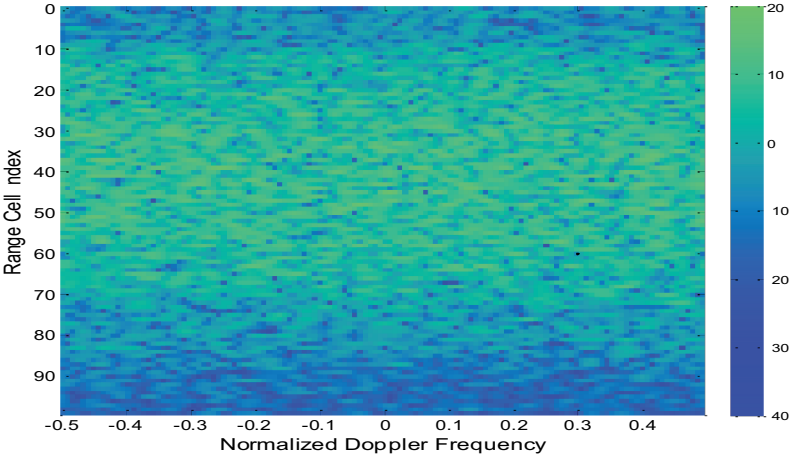

Figure 3. The estimation of the range-Doppler plane using the traditional matched filtering method.

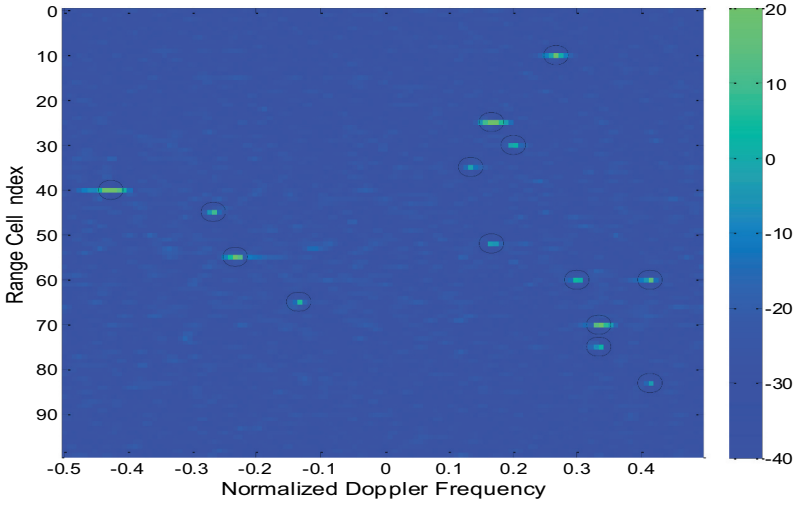

Figure 4. The estimation of the range-Doppler plane using the MAMPC method.

Secondly, the estimated range-Doppler plane by the MAMPC method is illustrated in Figure 4. The MAMPC method effectively estimates the range-Doppler plane for both the true and the false targets and suppresses the range-Doppler side-lobes. However, the method cannot distinguish between the true and false targets, and thus cannot suppress the deceptive false targets. Moreover, it is evident to see that the extension effect of the side-lobes of the deceptive false targets is significantly obvious than the true targets due to the large power of the false targets (JSR). But, the extension of the side-lobes cannot be used to discriminate and suppressed the deceptive false targets.

Thirdly, the estimation of the range-Doppler plane using the proposed method is shown in Figure 5. From Figure 5, it is observed that the proposed method successfully suppresses the false targets and maintains the true targets.

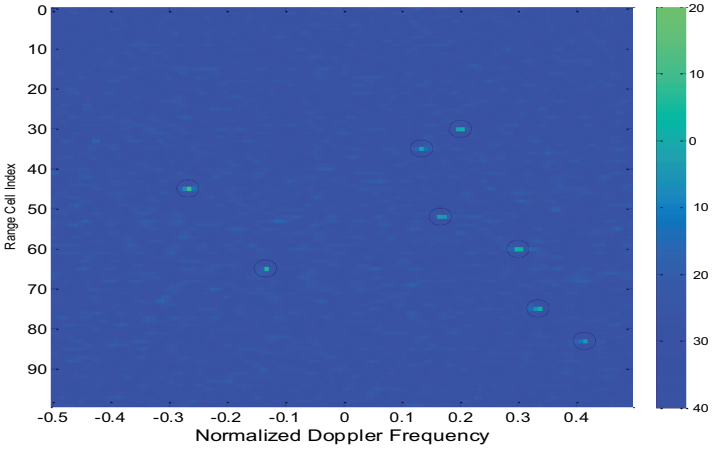

Figure 5. The estimation of the range-Doppler plane using the proposed method.

It is worth pointing out that the method estimates both the range-Doppler plane of the true and the false targets based on current and previous PRI due to the initial-phase difference. Therefore, an additional plot may be generated to improve the ability to distinguish between the true and deceptive false targets by plotting the estimated range-Doppler plane concerning the deceptive false targets (previous PRI). The estimation of the range-Doppler plane of the deceptive false targets is plotted in Figure 6. The result indicates that the range-Doppler plane of the false targets is also estimated and can use for improving the suppression or for other purposes.

Finally, we analyse the mean square error (MSE) performance of the estimation of true targets, which assess the performance of the proposed algorithm for estimating the range-Doppler plane of the true targets and suppressing the false targets. The same parameter simulations are used with 200 Monte Carlo trails.

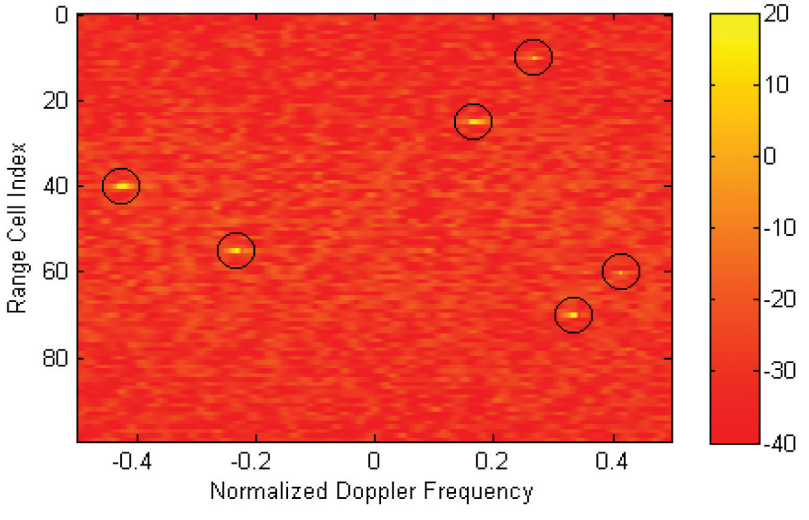

Figure 6. The estimation of the range-Doppler plane of the deceptive false targets.

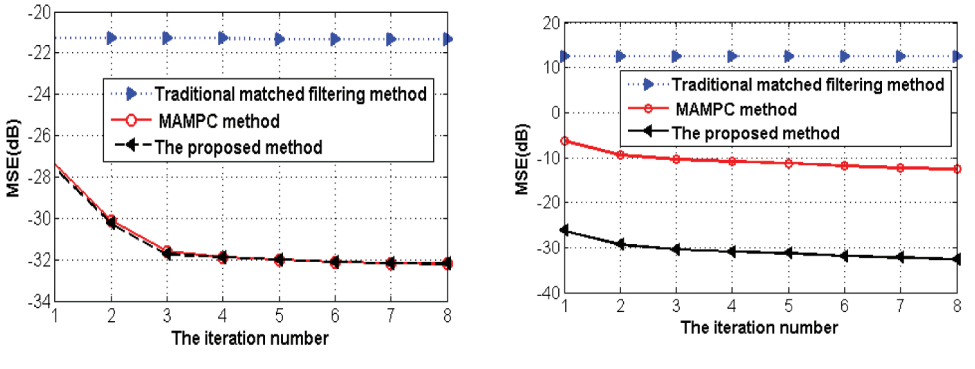

Figure 7. The MSE versus iteration number (a) In the scenario without the deceptive false targets (b) In the scenario with the deceptive false targets targets.

Table 3. Iterations Number performance Comparison.

Iteration number (Q)	MSE (dB)	Elapsed Time (sec)
1	−27.6	18.132
5	−32.1	22.566
10	−32.4	29.123
15	−34	37.346
20	−36	44.256
25	−39.5	56.265

In Figure 7, we plot the MSE curves of the range-Doppler plane estimation of true targets versus iteration number in the scenarios with and without the deceptive false targets, exploiting the traditional matched filtering method, MAMPC method, and the proposed method. Figure 7(a) shows the range-Doppler plane estimation of the true targets in the scenario without the deceptive false targets, whereas Figure 7(b) shows the range-Doppler plane estimation in the presence of the deceptive false targets.

It is evident from Figure 7(a) that in the scenario without the deceptive false jamming, the performance of the MAMPC method and the proposed method almost identical and they outperform the traditional matched filtering method. These results are reasonable because the traditional matched filtering method is not good at estimating the range-Doppler plane of the true targets, and the MAMPC method in the absence of the deceptive false targets can estimate the range-Doppler plane of the true targets effectively. However, in the scenario with deceptive false targets, as shown in Figure 7 (b), the traditional matched filtering method and MAMPC method highly influenced and their performance degraded dramatically. The MAMPC method could not distinguish the range-Doppler plane of the true targets from the false ones at the output of the processor. In contrast, since the true and false targets can be distinguished by introducing the random initial phases, the proposed approach performs well in the scenarios with or without the deceptive false targets. Therefore, the proposed approach can suppress deceptive jamming effectively.

To show the effectiveness of adaptive iterative filter for mitigating the MSE in range Doppler dimension in our method, we compare the MSE versus the number of iterations and the elapsed time in Table 3. It is clear to see that form Table 3 the large number of iterations can mitigate the MSE in range-Doppler dimension. Nevertheless, with high computational complexity. It is worth highlighting that for the aforementioned figures we set the number of iterations to be eight (Q = 8) and the sampling number in the range and Doppler dimensions used were G = 32 and U = 128 respectively. Actually, they are sufficiently large. Thus, to achieve a good trade-off between suppression performance and computational complexity the mentioned parameters can be further reduced.

5. Conclusion

An efficient anti-hamming method has been presented for countering the range-velocity deceptive jamming in PD radar. The presented method realised on the adaptive filtering algorithm and benefitting from the transmitted pulses with random initial phases, where at the current PRI, the DRFM jammer transmits the previous pulse that has been used by the radar. The estimation is carried out to the range-Doppler plane of the true targets in range dimension and Doppler dimension after obtaining the whole range-Doppler plane

sampling results of both the real targets and the deceptive false targets. The numerical results verified the validity and the efficiency of the anti-jamming method and proved that it can achieve superior performance compared to MAMPC and the traditional matched filter method.

Disclosure statement

No potential conflict of interest was reported by the author(s).

Funding

This work was supported in part by the National Natural Science Foundation of China under [Grant 61472066], Sichuan Science and Technology Program [No. 2018GZ0180, 2018GZ0085, 2017GZDZX0001, 2017GZDZX0002].

ORCID

Mohammed Ramadan http://orcid.org/0000-0003-3105-3079

References

Abdalla, A., Abdalla, H., Ramadan, M., Mohamed, S., & Bin, T. (2017). Overview of frequency diverse array in radar ECCM applications. In *2017 International Conference on Communication, Control, Computing, and Electronics Engineering (ICCCCEE)* (p. 5). Khartoum. https://doi.org/10.1109/ICCCCEE.2017.7867610

Abdalla, A., Wang, W. Q., Yuan, Z., Mohamed, S., & Bin, T. (2016). Subarray-based FDA radar to counteract deceptive ECM signals. *EURASIP Journal on Advances in Signal Processing*, *104*, 1–11. https://doi.org/10.1186/s13634-016-0403-6

Abdalla, A., Yuan, Z., & Bin, B. (2016). ECCM schemes in netted radar system based on temporal pulse diversity. *Journal of Systems Engineering and Electronics*, 27(5), 1001–1009. https://doi.org/10. 21629/JSEE.2016.05.08

Abdalla, A., Yuan, Z., Longdon, S. N., Bore, J. C., & Bin, T. (2015). A study of ECCM techniques and their perf ormance. In *2015 IEEE International Conference on Signal Processing, Communications, and Computing (ICSPCC)* (pp. 1–6). Ningbo. https://doi.org/10.1109/ICSPCC 2015.7338885

Abdalla, A., Yuan, Z., Ramadan, M., & Bin, T. (2015). An improved radar ECCM method based on orthogonal pulse block and parallel matching filter. *Journal of Communications*, *10*(8), 610–614. https://doi.org/10.12720/jcm.10.8.610-614

Ahmed, A., Shokrallah, A. M. G., Yuan, Z. H. A. O., Ying, X., & Bin, T. A. N. G. (2018, April). Deceptive jamming suppression in multistatic radar based on coherent clustering. *Journal of Systems Engineering and Electronics*, 29(2), 269–277. https://doi.org/10.21629/JSEE.2018.02.07

Akhtar, J. (2009). Orthogonal block coded ECCM schemes against repeat radar jammers. *IEEE Transactions on Aerospace and Electronic Systems*, 45(3), 1218–1226. https://doi.org/10.1109/ TAES.2009.5259195

Bandiera, F., Besson, O., & Ricci, G. (2008). An ABORT-like detector with improved mismatched signals rejection capabilities. *IEEE Transactions on Signal Processing*, 56(1), 14–25. https://doi.org/10.1109/TSP.2007.906690

Berger, S. D. (2003, April). Digital radio frequency memory linear range gate stealer spectrum. *IEEE Transactions on Aerospace and Electronic Systems*, 39(2), 725–735. https://doi.org/10.1109/TAES.2003.1207279

Bokov, A., Vazhenin, V., & Zeynalov, E. (2019). Development and evaluation of the universal DRFM-based simulator of radar targets. In *2019 International Multi-Conference on Engineering, Computer and Information Sciences (SIBIRCON)* (pp. 0182–0186). Novosibirsk, Russia. https://doi.org/10.1109/SIBIRCON48586.2019.8958398

Cui, G., Yang, Y, Zhao, H, Iommelli, S., & Yu, X. (2017). An adaptive sequential estimation algorithm for velocity jamming suppression. *Signal Processing*, *134*, 70–75. https://doi.org/10.1016/j.sigpro.2016.11.012

Haykin, S. (2006). Cognitive radar: A way of the future. *IEEE Signal Processing Magazine*, 23(1), 30–40. https://doi.org/10.1109/MSP.2006.1593335

Kelly, E. J. (1986, March). An adaptive detection algorithm. *IEEE Transactions on Aerospace and Electronic Systems*, AES-22(2), 115–127. https://doi.org/10.1109/TAES.1986.310745

Liang, J., Zeng, X., Wang, W., Chen, H. (2011). L-shaped array-based elevation and azimuth direction finding in the presence of mutual coupling. *Signal Processing*, 91(5), 1319–1328. https://doi.org/ 10.1016/j.sigpro.2010.12.001

Liu, W., Meng, J., & Zhou, L. (2019). Impact analysis of DRFM-based active jamming to radar detection efficiency. *The Journal of Engineering*, 2019(20), 6856–6858. https://doi.org/10.1049/joe.2019. 0501 10

Liu, Z., Sui, J., Wei, Z., & Li, X. (2018). A sparse-driven anti-velocity deception jamming strategy based on pulse-Doppler radar with random pulse initial phases. *Sensors*, 18(4), 1249. https://doi.org/10.3390/s18041249

Maini, A. K. (2018). Electronic warf are. In *H andbook of defence electronics and optronics: Fundamentals, technologies, and systems* (pp. 475–554). Wiley. https://doi.org/10.1002/9781119184737

Mandal, A., & Mishra, R. (2017). Digital equalization for cancellation of noise-like interferences in adaptive spatial filtering. *Circuits, Systems, and Signal Processing*, 36(2), 675–702. https://doi.org/ 10.1007/s00034-016-0324-5

Mesarcik, M. B., O'Hagan, D. W., & Paine, S. (2019). Low-cost FPGA based implementation of a DRFM system. In *2019 IEEE Radar Conference (RadarConf)* (pp. 1–6). Boston, MA. https://doi.org/10.1109/RADAR.2019.8835754

Richards, M. A., Scheer, J. A., & Holm, W. A. (2010). *Principles of modern radar: Basic principles*. Sci-tech.

Wen, C., Huang, Y., Wu, J., Peng, J., Zhou, Y., & Liu, J. (2019). Cognitive anti-deception-jamming for airborne array radar via phase-only pattern notching with nested ADMM. *IEEE Access*, *7*, 153660–153674. https://doi.org/10.1109/ACCESS 2019.2948507

Xiong, W., Wang, X., & Zhang, G. (2016). Cognitive wavef orm design for anti-velocity deception jamming with adaptive initial phases. In *2016 IEEE radar conference* (pp. 1–5). Philadelphia, USA.

Xu, J., Kang, J., Liao, G., & So, H. C. (2018). Mainlobe deceptive jammer suppression with FDA-MIMO radar. In *2018 IEEE 10th Sensor Array and Multichannel Signal Processing Workshop (SAM)* (pp. 504–508). Sheffield. https://doi.org/10.1109/SAM 2018.8448961

Yan, L., Addabbo, P., Hao, C., Orlando, D., & Farina, A. (2020, April). New ECCM techniques against noise-like and/or coherent interferers. *IEEE Transactions on Aerospace and Electronic Systems*, 56 (2), 1172–1188. https://doi.org/10.1109/TAES.2019.2929968

Yang, Y., Cui, C., and Zhao, H., et al. (2015, May). Optimized phase-coded waveform design against velocity deception. In *In the proceedings of the IEEE radar conference* (pp. 400–404). Arlington, VA, USA.

Yang, Y., Li, L., Cui, G., Yi, W., Kong, L., & Yang, X. (2015). A modified adaptive multi-pulse compression algorithm for fast implementation. In *Proceedings of the international IEEE radar conference* (pp. 0390–0394). Arlington, VA, USA.

Yu, H., Liu, N., Zhang, L., Li, Q., Zhang, J., Tang, S., & Zhao, S. (2020, August). An interference suppression method f or multistatic radar based on noise subspace projection. *IEEE Sensors Journal*, 20(15), 8797–8805. https://doi.org/10.1109/JSEN.2020.2984389

Yu, X., Cui, G., and Yang, Y., et al. (2018). Fast implementation f or modif ied adaptive multi-pulse compression. *EURASIP Journal on Advances in Signal Processing*, *2016*(127), 1–12. https://doi.org/10.1186/s13634-016-0423-2

Yu, Y., Yang, T., Chen, H., Lamare, R. C. D., & Li, Y. (2021). Sparsity-aware SSAF algorithm with individual weighting factors: Performance analysis and improvements in acoustic echo cancellation. *Signal Processing*, *178*, 107806. https://doi.org/10.1016/j.sigpro.2020.107806

Zhang, G., Huang, T., Liu, Y., Eldar, Y. C., & Wang, X. (2019). Frequency agile radar using atomic norm soft thresholding with modulations. In *2019 IEEE Radar Conference (RadarConf)* (pp. 1–6). Boston, MA, USA. https://doi.org/10.1109/RADAR.2019.8835847

Zhang, J., Zhu, D., & Zhang, G. (2013, April). New anti-velocity deception jamming technique using pulses with adaptive initial phases. *IEEE Transactions on Aerospace and Electronic Systems*, 49(2), 1290–1300. https://doi.org/10.1109/TAES.2013.6494414

Zhang, S., Yang, Y., Cui, G., Wang, B., Ji, H., & Iommelli, S. (2016). Range-velocity jamming suppression algorithm based on adaptive iterative filtering. In *2016 IEEE Radar Conference (RadarConf)* (pp. 1– 6). Philadelphia, PA. https://doi.org/10.1109/RADAR.2016.7485305

Zhu, L. (2020). Selection of multi-level deep features via spearman rank correlation for synthetic aperture radar target recognition using decision fusion. *IEEE Access*, *8*, 133914–133927. https://doi.org/10.1109/ACCESS.2020.3010969